Geophysical Research Letters

RESEARCH LETTER
10.1029/2024GL109374

Constraining Regional Hydrological Sensitivity Over Tropical Oceans

Jie He[1], Yi Deng[1], Boniface Fosu[2,3], Yen-Heng Lin[3], and Kezhou Lu[1]

[1]School of Earth and Atmospheric Sciences, Georgia Institute of Technology, Atlanta, GA, USA, [2]Department of Geosciences, Mississippi State University, Mississippi State, MS, USA, [3]Northern Gulf Institute, Mississippi State University, Mississippi State, MS, USA

Key Points:

- Regional hydrological sensitivity is an important source of uncertainty in rainfall projections over tropical oceans
- Regional hydrological sensitivity can be constrained by components of rainfall-temperature relationship that stay constant during warming
- Uncertainty in regional hydrological sensitivity originates largely from surface convergence sensitivity to temperature gradient changes

Supporting Information:

Supporting Information may be found in the online version of this article.

Correspondence to:

J. He,
jie.he@eas.gatech.edu

Citation:

He, J., Deng, Y., Fosu, B., Lin, Y.-H., & Lu, K. (2024). Constraining regional hydrological sensitivity over tropical oceans. *Geophysical Research Letters*, *51*, e2024GL109374. https://doi.org/10.1029/2024GL109374

Received 22 MAR 2024
Accepted 13 AUG 2024

Abstract Regional hydrological sensitivity (i.e., precipitation change per degree local surface warming) contributes substantially to the uncertainty in future precipitation projections over tropical oceans. Here, we investigate the sensitivity of relative precipitation (P*, precipitation divided by the basin average precipitation) to local sea surface temperature (SST) change by dissecting it into three components, namely the sensitivity of P* to relative SST (SST_{rel}, SST minus the tropical mean SST) changes, the sensitivity of P* to surface convergence changes, and the sensitivity of surface convergence to SST gradient changes. We show that the relationships between P* and SST_{rel}, and between P*, surface convergence, and SST gradients are largely constant during climate change. This allows us to constrain regional hydrological sensitivity based on present-day SST-precipitation relationships. The sensitivity of surface convergence to SST gradient changes is a main source of uncertainty in regional hydrological sensitivity and is likely underestimated in GCMs.

Plain Language Summary Understanding how precipitation will change over tropical oceans is important because these changes influence the atmospheric circulation, which in turn affects the global climate and weather patterns. Climate models disagree on their projections of precipitation changes over tropical oceans in part due to a lack of understanding on how precipitation should respond to a given amount of local surface warming. We find that the sensitivity of precipitation to future changes in local sea surface temperature (which is commonly referred to as regional hydrological sensitivity) largely depends on the present-day relationship between precipitation and local sea surface temperature, as well as that between precipitation and the spatial gradient in sea surface temperature, and both relationships are observable and thus can serve as constraints. We find that inter-model differences in regional hydrological sensitivity result primarily from differences in the response of surface winds to sea surface temperature gradient changes.

1. Introduction

Tropical precipitation is a main component of the global hydrological cycle. Both tropical land and oceanic precipitation changes have far-reaching implications on the global climate system via atmospheric teleconnections (e.g., Chen et al., 2020; Lu et al., 2023). The projection of future tropical precipitation is highly uncertain at regional scales (Lee et al., 2021). The uncertainty in regional precipitation over tropical oceans is often attributed to the uncertainty in sea surface temperature (SST) changes (Kent et al., 2015; Ma & Xie, 2013), because precipitation changes spatially follow local SST changes (S.-P. Xie et al., 2010). But SST is only half of the equation. Chadwick (2016) showed that a considerable portion of the inter-model spread in tropical precipitation changes persist when the models are driven by the same SST changes (Figures 1a and 1b). This suggests that the uncertainty in regional precipitation changes (δP) is not only associated with local SST changes (δSST), but likely precipitation sensitivity to local SST changes (δP/δSST) as well. However, regional hydrological sensitivity (which describes precipitation change per degree local surface temperature change) has not been thoroughly studied.

On the other hand, there has been great interest surrounding the global and tropical mean hydrological sensitivity due to its substantial variance among climate models (DeAngelis et al., 2015; Su et al., 2017; Watanabe et al., 2018; J. Zhang & Huang, 2023). The tropical mean hydrological sensitivity (often calculated as the percentage change in tropical mean precipitation per degree tropical mean surface warming) varies by roughly a factor of three among the Coupled Model Intercomparison Project (CMIP) models (He & Soden, 2015). Means to constrain the projected tropical mean hydrological sensitivity have been explored in recent studies (Ham

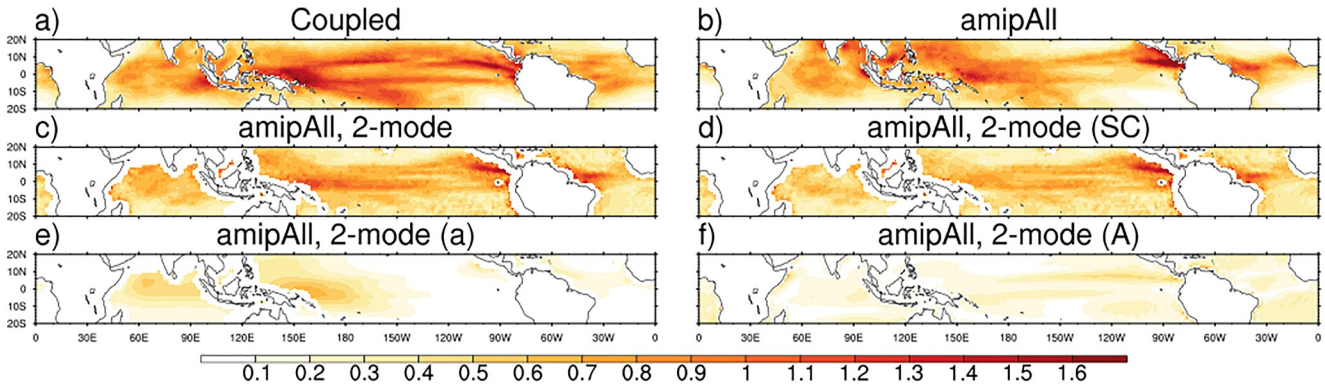

Figure 1. Inter-model standard deviation of precipitation changes (in mm/day) from the coupled 1pctCO2 (a) and uncoupled amipAll (b) simulations and the 2-mode model based on changes in the amipAll simulation (c)–(f). Panel c represents the total inter-model spread captured by incorporating inter-model variations in all parameters and input variables in the 2-mode model. Panels d represents the inter-model spread associated with SC by only incorporating inter-model variations in SC while setting all other components of the 2-mode model (including parameters a and A) to their corresponding multi-model mean values. Panels e and f are the same as d except that they represent the inter-model spread associated with parameter a and A, respectively.

et al., 2018; Park et al., 2022). In comparison, regional hydrological sensitivity has received far less attention. However, because the broader impacts of tropical precipitation changes depend more on the regional distribution rather than the tropical mean of such changes (Lu et al., 2023), understanding regional hydrological sensitivity is important from both scientific and pragmatic points of view.

While regional hydrological sensitivity to future warming has been underexplored, it is useful to review precipitation sensitivity to internal SST variations, where climate models were found systematically biased (Good et al., 2020). Because internal precipitation variability is driven by a multitude of factors, a major challenge in quantifying precipitation sensitivity to internal SST variability is to derive a physically meaningful relationship between precipitation anomalies and SST anomalies (Graham & Barnett, 1987; Lau et al., 1997; C. Zhang, 1993). He et al. (2018) found that the equations that determine precipitation sensitivity to internal SST variability are the same as those governing the climatological mean SST-precipitation relationship. This means that the response of precipitation per degree internal SST variation is determined by the variation in climatological precipitation per degree climatological SST variation (i.e., the slope of climatological precipitation in SST space, Figures 2a and 2b). The implication of such a finding is that during internal climate variations, changes in SSTs result in a geographical reshuffling of convective and non-convective areas while the SST-precipitation relationship remains constant. This allows us to constrain models' precipitation sensitivity to internal SST anomalies by using the observed climatological SST-precipitation relationship.

Although precipitation responds differently to internal and anthropogenic SST variations (e.g., Kramer & Soden, 2016), it has been reported that certain aspects of SST-precipitation relationship should remain constant during climate change. For example, Johnson and Xie (2010) examined the tropical mean SST-precipitation relationship and argued that the present-day and future relationship between precipitation and relative SST (SST_{rel}, defined as SST minus the tropical mean SST) is roughly the same (their Figure 3a). But this gets complicated when the three tropical basins are examined separately. As shown in Figures 2a and 2b, the SST_{rel}-precipitation relationship is different and responds differently to warming among the three basins.

Why does the SST_{rel}-precipitation relationship vary among regions and what drives its future changes? Because the upper tropospheric temperature is largely uniform in the tropics, changes in precipitation are determined predominantly by local changes in boundary-layer moist static energy (MSE0, Xie et al., 2010). Given the fact that the upper troposphere warms commensurately with the tropical mean MSE0 changes (Johnson & Xie, 2010), one may expect a constant relationship between precipitation and relative MSE0 ($MSE0_{rel}$, i.e., MSE0 scaled by the tropical mean MSE0) under warming, which has been identified in GCMs (He, Lu, et al., 2024). Because $MSE0_{rel}$ is essentially a function of SST_{rel} and boundary-layer relative humidity (RH0), and given the constancy in the $MSE0_{rel}$-precipitation relationship, spatial variations and future changes in the SST_{rel}-precipitation relationship are determined by RH0. Inter-basin differences in RH0 changes resulting largely from land-sea moisture transport cause diverging hydrological sensitivity among tropical basins (He, Lu, et al., 2024). The effect of this

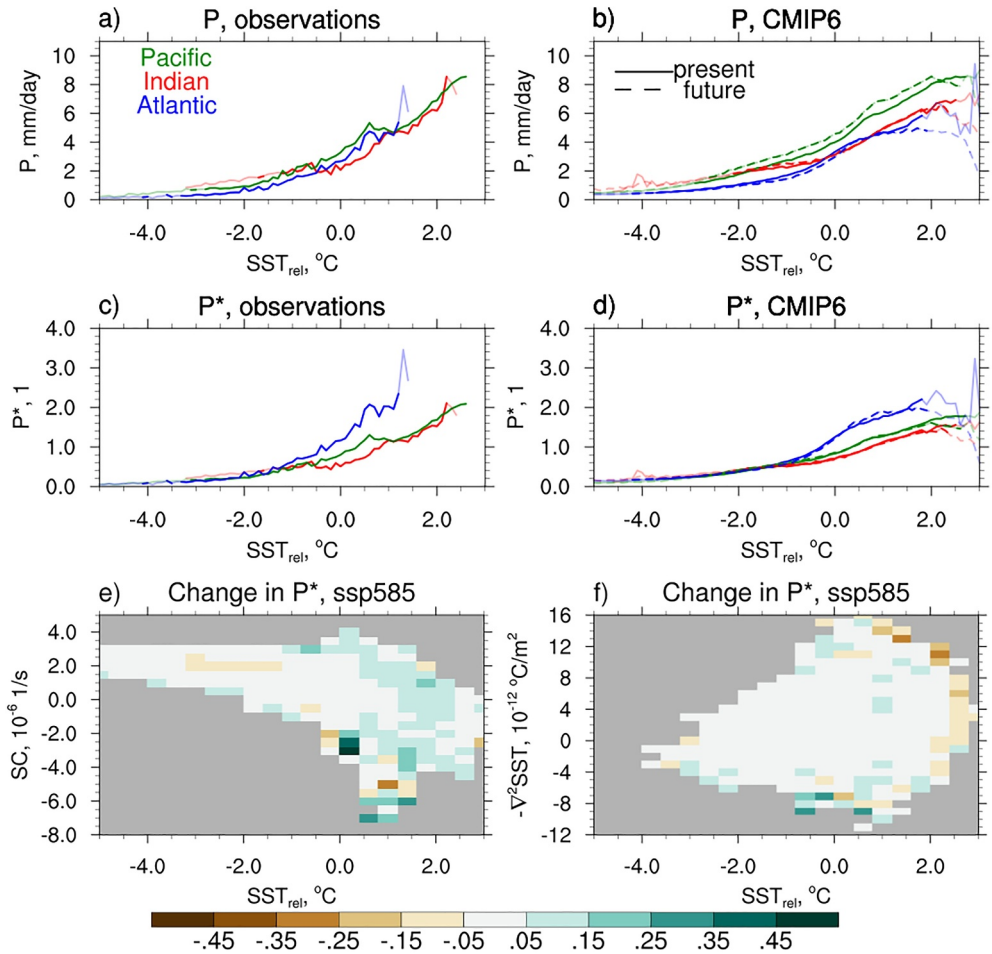

Figure 2. (a)-(b) Basin precipitation averaged for 0.1 SST_{rel} bins from observations (a) and CMIP6 multi-model mean historical and ssp585 simulations (b). SST_{rel} bins that account for less than 0.5% of the basin area are shown in semitransparent colors. (c)-(d) Same as (a)-(b) but for relative precipitation. (e)-(f) ssp585 multi-model mean changes in relative precipitation (unit: 1) as a function of SST_{rel} and SC (e) and as a function of SST_{rel} and $-\nabla^2 SST$ (f). Panels e and f use the same colorscale as that in Figure 4.

on the SST_{rel}-precipitation relationship can be accounted for by considering relative precipitation (P*, i.e., P divided by the basin mean P), which appears constant with warming in SST_{rel} space (Figure 1d). Within each basin, changes in surface convergence (SC) resulting from SST gradient changes (Duffy et al., 2020) drive RH0 changes and thus determine the sensitivity of P* to local sea surface warming (see Figure S1 in Supporting Information S1, adapted from He, Lu, et al., 2024).

Therefore, the SST_{rel}-P* relationship and its future changes can be understood by analyzing changes in the interactions between SST_{rel}, SC, and P*. Specifically, both SST_{rel} and SC affect P*, and SST_{rel} affects SC via the formation of SST gradients (Back & Bretherton, 2009b; Lindzen & Nigam, 1987) – all three processes are incorporated into the SST_{rel}-P* relationships shown in Figures 2c and 2d. Here, we aim to quantify these processes by using a 2-mode model where precipitation is expressed as a function of SST and SC, and the latter is linked to SST gradients (Back & Bretherton, 2009a; Duffy et al., 2020). We hypothesize that the effects of SST_{rel} and SC on P* and the effects of SST gradients on SC do not change under warming. If valid, this would allow us to constrain regional hydrological sensitivity based on the present-day SST-precipitation relationship.

In this paper, we first describe a modified version of the 2-mode model (Section 3), which allows us to delineate regional hydrological sensitivity by partitioning it into three components, namely, (a) sensitivity of P* to SST_{rel} changes ($\partial P^*/\partial SST_{rel}$), (b) sensitivity of P* to SC changes ($\partial P^*/\partial SC$), and (c) sensitivity of SC to SST gradient

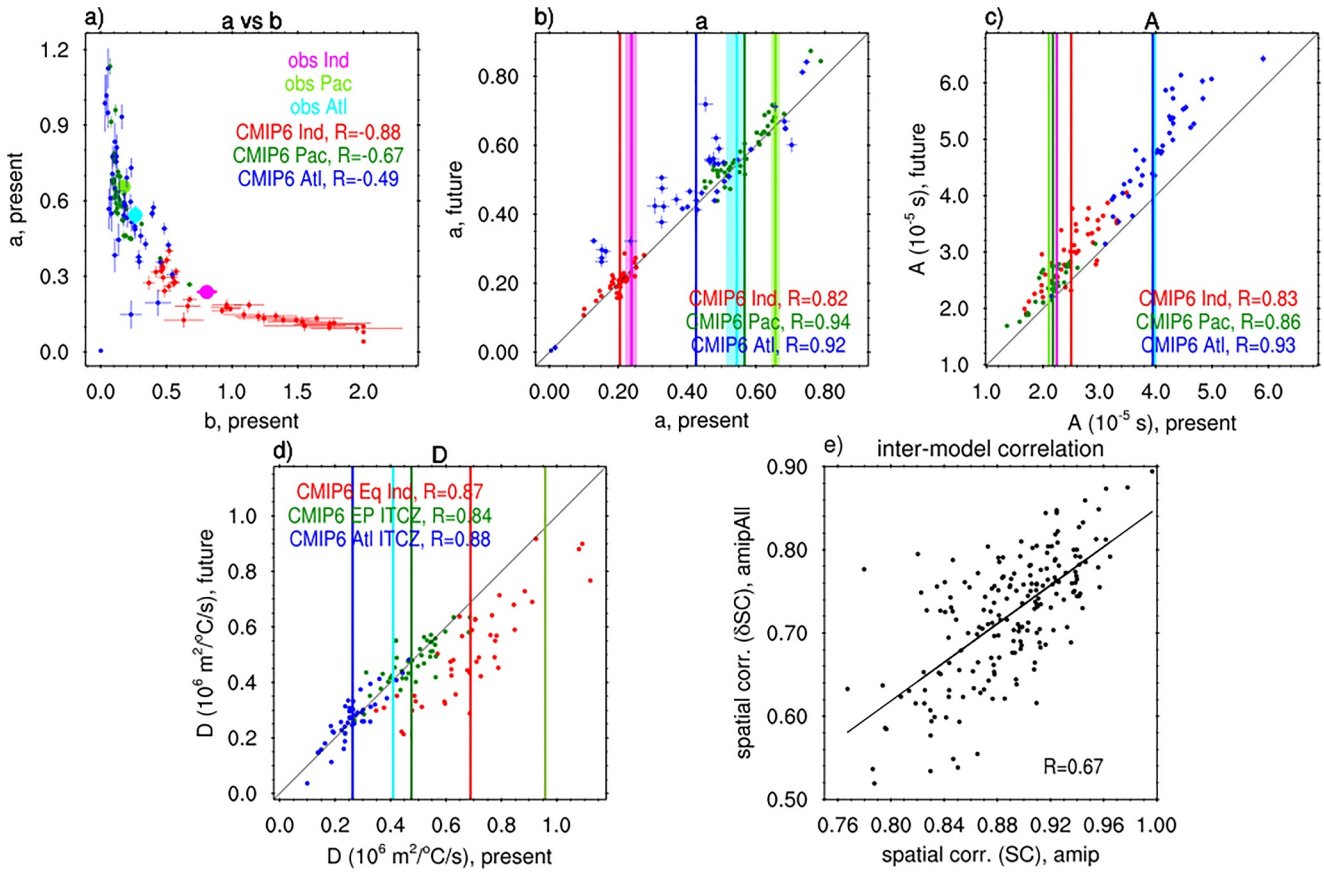

Figure 3. Relationships between present-day *a* and *b* (a), present-day and future *a* (b), present-day and future *A* (c), present and future *D* (d) based on the historical and ssp585 simulations. Small dots represent individual GCMs and vertical lines in corresponding colors represent the multi-model mean. Inter-model correlation coefficients are shown by texts. Observations are represented by the large dots in panel a and by vertical lines in panels b, c, and d in lighter colors. The 95% uncertainty range is represented by the crosses for the individual GCMs in a-c and observations in panel a and is represented by the semitransparent shading for the observations in b-c. In panel d, the observed D values for the South Equatorial Indian Ocean and the eastern Pacific ITCZ region are virtually identical, both at roughly 0.95. Panel e is a scatter plot of the inter-model spatial correlation of present SC (*x*-axis) and that of SC changes (*y*-axis) over tropical oceans based on the uncoupled simulations.

changes. We then examine components (a) and (b) in Section 4 and component (c) in Section 5. The implications and limitations of our results will be discussed in Section 6.

2. Data

We use monthly data from observations and CMIP simulations. All data sets are interpolated onto a common 1° by 1° horizontal grid and a 19-level pressure coordinate before they are analyzed.

The observed SST data is a merged product based on the Hadley Center SST data set version 1 and the National Oceanic and Atmospheric Administration optimum interpolation SST analysis version 2 (Hurrell et al., 2008). The data ranges from 1979 to 2021 and is archived at 1° resolution. To account for the uncertainty in individual precipitation observations, we average three widely used precipitation data sets: (a) the Global Precipitation Climatology Project (GPCP) data version two from 1979 to 2021 at 2.5° resolution (Adler et al., 2003), (b) the Climate Prediction Center Merged Analysis of Precipitation (CMAP) data from 1979 to 2021 at 2.5° resolution (P. Xie & Arkin, 1997), and (c) the Tropical Rainfall Measuring Mission Project (TRMM) 3B43 data version 7 from 1998 to 2019 at 0.25° resolution (Huffman et al., 2010).

We use 3D atmospheric variables, including horizontal and vertical winds, air temperature and geopotential height from reanalysis data during the period of 1979–2021. To minimize the effect of uncertainty within individual data sets, we average three widely used reanalysis data sets: (a) ERA5 (the fifth generation of the European

Center for Medium-Range Weather Forecasts reanalysis) on a 30 km horizontal grid and 137 vertical levels (Hersbach et al., 2020), (b) NCEP/DOE-II (the National Center for Environmental Prediction and Department of Energy Reanalysis II) at 2.5° resolution with 17 vertical levels (Kanamitsu et al., 2002), and (c) JRA-55 (the Japanese 55-year Reanalysis) at roughly 1° resolution with 37 vertical levels (KOBAYASHI et al., 2015).

We analyze the historical and ssp585 simulations from 43 CMIP6 models. We use the last 30 years (1985–2014) of the historical simulation to evaluate models against observations and to provide a baseline for future changes. The projected future climate is calculated based on the last 30 years (2071–2100) of the ssp585 simulation, which represents the upper boundary of the range of emission scenarios included in CMIP6 (Eyring et al., 2016).

In Figure 1a, the coupled precipitation changes are calculated as the difference between year 121–150 and year 1–30 of the 1pctCO2 simulation, where the atmospheric CO_2 concentration increases at 1% per year starting from the pre-industrial level. To exclude the effect of inter-model differences in SSTs, we also analyze uncoupled atmosphere-only simulations where SSTs are kept the same across models. We use the amip simulation as the uncoupled baseline, which is driven by observed (1979–2014) monthly SST and sea ice concentrations. The uncoupled future simulation (amipAll) contains rising CO_2 and projected changes in SST (from CMIP3, 1pctCO2) on top of the baseline. amipAll is constructed by linearly combining the amip-4 x CO2 and amip-future4K simulations scaled to match the CO_2 forcing in the 1pctCO2 simulation, following He, Lu, et al. (2024). Nine CMIP5 models and 11 CMIP6 models are used for the 1pctCO2 and uncoupled simulations. Table S1 in Supporting Information S1 lists the models and the realizations analyzed.

3. 2-Mode Model

We apply a 2-mode model to dissect precipitation driven by SST amplitude and SST gradient. The 2-mode model was originally created by Back and Bretherton (2009a). "2-mode" refers to the fact that most of tropical precipitation is associated with either a shallow or a deep vertical velocity profile (Figure S2 in Supporting Information S1). The shallow mode features maximum updraft in the boundary layer. The bottom-heavy structure is associated with strong boundary layer wind convergence which is driven by low-level pressure gradients that result from the gradients of the underlying SSTs (Back & Bretherton, 2009b; Lindzen & Nigam, 1987). The shallow mode is the main form of precipitation in the Eastern Pacific convergence zone where SST gradients are sharp. The deep mode peaks in the upper troposphere and can be attributed to atmospheric instability driven by a high amount of near surface moist static energy (MSE, Back & Bretherton, 2009a). It is therefore strongest in the warm pool regions but can also be affected by SST gradients, which influence low-level MSE by generating moisture convergence (Duffy et al., 2020). In the 2-mode model, the effect of SST gradients is often represented by boundary-layer wind convergence (i.e., SC, calculated as $-\nabla(u_{925hPa}, v_{925hPa})$, where u_{925hPa} and v_{925hPa} are 925 hPa horizontal winds) rather than SST gradients themselves (i.e., $-\nabla^2$SST) due to the spatial noisiness in the latter. While SC is predominantly driven by SST gradients (Back & Bretherton, 2009b), the two do not align perfectly (Figure S3 in Supporting Information S1). Here, the 2-mode model is used to attribute precipitation to SST and SC, and link between SC and SST gradients will be discussed separately in Section 5.

Our 2-mode model largely follows that of Duffy et al. (2020), but with the incorporation of inter-basin differences in SST-precipitation relationships which lead to substantial error reduction. We will use the 2-mode model to simulate P*, which is the constrainable component of tropical precipitation changes (as we will later show). The main steps of the 2-mode model are outlined below. We direct the readers to Back and Bretherton (2009a) and Duffy et al. (2020) for details of the calculation, while pointing out the modifications made herein.

Tropical precipitation at the regional scale is balanced mainly by the column integrated vertical advection of dry static energy (Back & Bretherton, 2009a):

$$LP^* = \left\langle \omega \frac{\partial s}{\partial p} \right\rangle \Big/ [P] + r \tag{1}$$

where L is the latent heat of condensation, P is precipitation, P^* is relative precipitation (i.e., P divided by the basin mean precipitation, $[P]$), ω pressure velocity, s dry static energy, p pressure, and $< >$ a pressure weighted vertical integral over an atmospheric column. The residual term (r) represents the sum of horizontal advection of s, eddy transport of s, surface sensible heat flux, and the atmospheric radiative cooling (i.e., the difference

between surface and top of the atmosphere radiation), all normalized by $[P]$. r has little spatial variation and is roughly equal to 1.

Equation 1 links precipitation to vertical velocity (ω); the latter is dissected into a deep mode (subscript d) and a shallow mode (subscript s):

$$\omega \approx o_d\Omega_d + o_s\Omega_s \tag{2}$$

where $\Omega(p)$ describes the vertical profiles of each mode and $o(x,y,t)$ describes the spatial and seasonal variation. The deep and shallow modes are determined based on a linear combination of the first two EOF modes of ω, while ensuring that the shallow mode has zero surface convergence and the deep mode is orthogonal to the shallow mode (Back & Bretherton, 2009a).

Following previous 2-mode models, we also separate r into deep and shallow modes by linear multiple regression:

$$r \approx o_dR_d + o_sR_s + R_0 \tag{3}$$

where R_d, R_s, and R_0 are constant regression coefficients. While it is unclear how r is physically linked to o_d and o_s, Equation 3 is calculated solely for the mathematical purpose that both terms on the rhs of Equation 1 are dissected into deep and shallow modes. Combining Equations 1–3 yields the deep and shallow modes of P^*: $LP^* \approx LP^*_d + LP^*_s + R_0$, where $LP^*_d = \left(\left\langle\Omega_d\frac{\partial s}{\partial p}\right\rangle\Big/[P] + R_d\right)o_d$ and $LP^*_s = \left(\left\langle\Omega_s\frac{\partial s}{\partial p}\right\rangle\Big/[P] + R_s\right)o_s$. Spatial patterns of the deep and shallow precipitation are shown in Figure S4 in Supporting Information S1.

The shallow mode of P^* is related to SC by linear regression:

$$P^*_s \approx A_sSC + C_s \tag{4}$$

where A_s and C_s are regression coefficients.

The deep mode of P* is related to SST amplitude and SC by multiple regression

$$P^*_d \approx b \times \exp(a \times SST_{rel}) + A_dSC + C_d \tag{5}$$

where a, b, A_d and C_d are regression coefficients, determined via a nonlinear least squares analysis based on the trust region method (Conn et al., 2000). Note that SST_{rel} and SC are spatially correlated (at roughly 0.6 in observation/reanalysis and CMIP6 models), which likely affects the partition of P_d. We consider this an important limitation of the 2-mode model and will discuss its implications in Section 6.

Previous 2-mode models assumed that the SST_{rel}-driven P_d is zero below a certain SST threshold and grows linearly with SST above the threshold. This appears somewhat inconsistent with the actual SST-P relationship, which shows gradual and nonlinear precipitation growth throughout the SST space (Figures 2a and 2b). Therefore, we use an exponential function (i.e., $b \times exp\ (a \times SST_{rel})$) to represent the SST_{rel}-driven P_d. On the other hand, we are dealing with two SST_{rel} parameters (i.e., a and b). The two parameters both contribute positively to the SST_{rel}-driven P_d but are negatively correlated among models (Figure 3a). The way a and b are correlated indicates that this may be an artifact of the fitting process and that the two parameters may provide similar functionalities. To simplify the interpretation of the parameters, we set b constant while only allowing a to vary among models. Specifically, we estimate both a and b for the observations. But for CMIP6 models, b is prescribed for each basin as the observed values for both present-day and future simulations. This is consistent with Good et al. (2020) who applied a similar exponential function and proposed that precipitation sensitivity to SST should be represented by the coefficient within the exponent. Nevertheless, whether a or b is made the effective SST_{rel} parameter does not affect our conclusions.

The main modification with respect to previous 2-mode models is that the partition of deep and shallow modes (Equations 2 and 3) and the subsequent attribution to SST_{rel} and SC (Equations 4 and 5) are done separately for each basin rather than the entire tropical oceans. This is motivated by the fact that the three tropical basins have different SST-precipitation relationships (Figures 2a–2d). This results primarily from the basins' interaction with

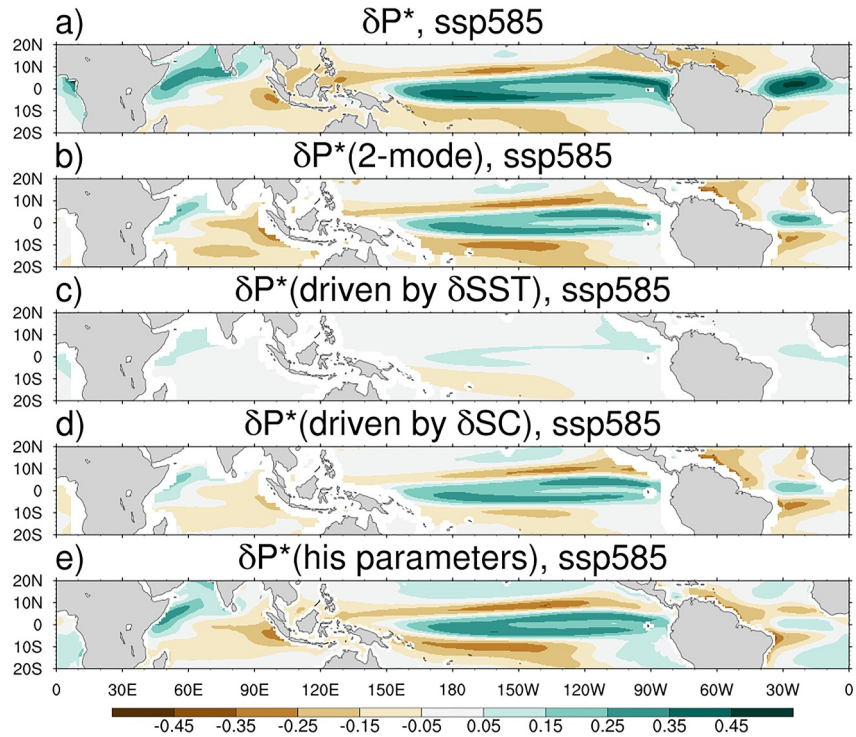

Figure 4. (a)-(b) ssp585 multi-model mean P* changes from GCMs (a) and the 2-mode model (b). (c)-(d) Multi-model mean P* changes due to changes in SST (c) and SC (d) from the 2-mode model. (e) Multi-model mean P* changes from the 2-mode model by using GCMs' historical parameters (e).

nearby land, which causes inter-basin differences in boundary-layer humidity and ultimately, differences in boundary-layer MSE for a given SST (He, Lu, et al., 2024). Consequently, the three basins have different profiles of deep and shallow convection (Figure S2 in Supporting Information S1) and yield different coefficients in the 2-mode model (Figure 3a). With the addition of inter-basin variations, the rmse for the estimated observed precipitation is substantially reduced to 0.89 mm/day, compared to that of 2.30 mm/day in Back and Bretherton (2009a) and 2.08 mm/day in Duffy et al. (2020). This suggests that incorporating regional variations in boundary-layer moisture that cannot be accounted for by local SSTs and SC could increase the accuracy of the 2-mode model.

Next, we dissect P^* into components driven by SST_{rel} and SC:

$$P^* \approx P^*(SST) + P^*(SC) + C_d + C_s + R_0/L \quad (6)$$

where $P^*(SST) = b \times exp\ (a \times SST_{rel})$, and $P^*(SC) = (A_d + A_s)SC$. Note that the observed precipitation is partitioned by using atmospheric variables from reanalysis data. Therefore, inconsistencies between observation and reanalysis data may result in poor fitting and potential underestimations of parameters. On the other hand, the 2-mode model exhibits similar levels of accuracy when applied to observed and CMIP6 precipitation (Figure S5 in Supporting Information S1).

The 2-mode model captures the CMIP6 multi-model mean P^* changes reasonably well (Figures 4a and 4b). The most notable inconsistencies appear in the Equatorial regions, which is also an issue for the previous 2-mode model (Figure 2 of Duffy et al., 2020). Consistent with Duffy et al. (2020), SC plays a substantially greater role in the projected tropical precipitation changes than SST_{rel} (Figures 4c and 4d). Note that Duffy et al. (2020) attributed a portion of precipitation changes to the "wet-get-wetter" effect (their Figure 2d), which is absent here because we only consider changes in P^* rather than P.

4. Precipitation Sensitivity to Anthropogenic SST_{rel} and SC Changes

As shown in Figures 3b and 3c, the present and future values of 2-mode model parameters are similar in amplitude and highly correlated among GCMs. Parameter a tends to be slightly lower at present-day, while the opposite is true for parameter A ($A = A_d + A_s$). Nevertheless, the differences between present-day and future parameters are substantially smaller than the parameters themselves. In Figure 4e, we estimate P* changes by using the present-day parameters to calculate P* in both historical and ssp585 simulations. The resulting P* changes are very similar to those in Figure 4b, with some exceptions in the Atlantic basin. This means that the present-day and future P* can be estimated by the same 2-mode model with only differences in SST_{rel} and SC. Therefore, we can obtain P* sensitivity to local SST_{rel} and SC changes by calculating the SST_{rel} and SC derivatives of Equation 6: $\partial P^* / \partial SST_{rel} = ab \times \exp(a \times SST_{rel})$, and $\partial P^* / \partial SC = A$.

Because parameter b is constant across models, $\partial P^* / \partial SST_{rel}$ is a function of a and SST_{rel}. By comparing a of GCMs and observations, we find that $\partial P^* / \partial SST_{rel}$ is underestimated by most GCMs (Figure 3b). This is consistent with Good et al. (2020), who reported systematic underestimations of precipitation sensitivity to internal and seasonal SST variations by CMIP models. In addition, there is substantial inter-model variation in a. The uncertainty in a has greater impacts on $\partial P^* / \partial SST_{rel}$ at higher SSTs. For example, the Pacific $\partial P^* / \partial SST_{rel}$ varies by a factor of 1.7 among GCMs for $SST_{rel} = 0$ and a factor of 3.4 for $SST_{rel} = 2°C$ (equivalent to present-day SST of roughly 29°C).

The observational estimate of $\partial P^* / \partial SC$ is well represented by the CMIP6 multi-model mean (Figure 3c). While there are no systematic biases in $\partial P^* / \partial SC$, there is considerable inter-model variance. $\partial P^* / \partial SC$ varies by a factor of 2.1, 2.2, and 2.8 for the Indian, Pacific, and Atlantic basins, respectively.

5. Linking SC to SST Gradients

In the uncoupled simulations where SST changes are the same across models, inter-model differences in precipitation changes are entirely due to differences in regional hydrological sensitivity (i.e., δP/δSST). The 2-mode model captures most of the uncertainty in the uncoupled precipitation changes (compare Figures 1b and 1c). This allows us to attribute the inter-model differences in regional hydrological sensitivity to differences in $\partial P^* / \partial SST_{rel}$, $\partial P^* / \partial SC$, and the sensitivity of SC to SST gradient changes [that is, $\partial SC / \partial(-\nabla^2 SST)$] by perturbing one of these parameters at a time in the 2-mode model. Although $\partial P^* / \partial SST_{rel}$ and $\partial P^* / \partial SC$ vary substantially among GCMs, their contributions to the uncertainty in precipitation changes are small (Figures 1e and 1f). Most of the uncertainty in the uncoupled precipitation changes results from inter-model differences in $\partial SC / \partial(-\nabla^2 SST)$ (Figure 1d).

We now explore constraints on $\partial SC / \partial(-\nabla^2 SST)$. To reduce the spatial noisiness of -∇^2SST, we apply a nine-point smoothing, following previous studies (Back & Bretherton, 2009b; Duffy et al., 2020). The relationship between SC and $-^2$SST is complex. On the one hand, strong SC is generally located where $-\nabla^2$SST is large (e.g., the eastern Pacific ITCZ and the Atlantic ITCZ, Figure S3 in Supporting Information S1). On the other hand, the dissimilarity between SC and $-\nabla^2$SST is also evident. The spatial correlation between the observed two fields is negative at −0.19. This means that SC does not always respond to $-\nabla^2$SST locally and that $\partial SC / \partial(-\nabla^2 SST)$ cannot be summarized by a single parameter (unlike $\partial P^* / \partial SST_{rel}$ and $\partial P^* / \partial SC$).

Here, we focus on three regions, namely the South Equatorial Indian Ocean (Eq Ind, 10S-0, 50 E−100 E), the eastern Pacific ITCZ (EP ITCZ, 5 N–13 N, 180 E−90 W), and the Atlantic ITCZ (Atl ITCZ, 2 N–10 N, 40 W–10 W), which host the strongest SC in each basin (Figure S3 in Supporting Information S1). Because the present-day SC and $-\nabla^2$SST are generally aligned in these regions, it makes sense to calculate the ratio (D) between the regional average SC and $-\nabla^2$SST. The present and future values of D are roughly the same (Figure 3e), indicating a constant relationship between SC and $-\nabla^2$SST during climate change. In addition, the amplitude of D is substantially smaller compared to observations in all three regions, consistent with Good et al. (2020) who found systematic biases in the simulation of shallow convergence in CMIP models.

Next, we examine whether the present-day D can be used to directly constrain $\partial SC/\partial(-\nabla^2 SST)$. In the South Equatorial Indian Ocean, D and $\partial SC/\partial(-\nabla^2 SST)$ are uncorrelated (Figure S6a in Supporting Information S1), likely because changes in SC are spatially shifted with respect to changes in $-\nabla^2$SST (Figures S2e, S2f in Supporting Information S1). In the eastern Pacific ITCZ and the Atlantic ITCZ where changes in SC and $-\nabla^2$SST are better aligned, moderate correlations are found between D and $\partial SC/\partial(-\nabla^2 SST)$ (Figures S6b, S2c in Supporting Information S1). These results indicate the feasibility of using present D as a direct constraint of SC changes in certain regions but also point to the high degree of spatial complexity in $\partial SC/\partial(-\nabla^2 SST)$.

Finally, we attempt to provide a holistic perspective on this issue with Figure 3e. Specifically, we analyze inter-model spatial correlation of present-day SC in amip (x-axis) and that of projected SC changes in amipAll (y-axis). It shows that models with similar present-day SC tend to project similar SC changes when subject to the same SST and SST changes. This indicates that models' skillfulness in projecting SC responses to $-\nabla^2$SST changes likely depends on their ability to capture the present-day SC-∇^2SST relationship.

6. Conclusions and Discussions

Using a modified 2-mode model, we examine regional hydrological sensitivity by partitioning it into three components, namely $\partial P^*/\partial SST_{rel}$, $\partial P^*/\partial SC$, and $\partial SC/\partial(-\nabla^2 SST)$. Our results suggest that the relationships between P* and SST_{rel}, between P* and SC, and between SC and SST gradients remain largely constant during climate change. As a result, P* changes little in the SST_{rel}–SC space and SST_{rel}–∇^2SST space (compare Figures 2e and 2f with Figure 4a). This confirms our hypothesis that regional changes in P* result from the geographical reshuffling of SST_{rel} and SST gradients, while the fundamental relationships between SST_{rel} and P* and those between SST gradients and P* remain constant. Therefore, a model's present SST-P relationship is a primary indicator of the accuracy in its projected regional hydrological sensitivity. Our results show an underestimation of $\partial P^*/\partial SST_{rel}$ and likely $\partial SC/\partial(-\nabla^2 SST)$, consistent with the low precipitation sensitivity to seasonal and internal SST variations previously identified in CMIP models (Good et al., 2020).

In the 2-mode model, the SST-driven and SC-driven P_d is estimated by multiple regression. However, because SST_{rel} and SC are not entirely independent, the effects of SST amplitude and SC may not be cleanly separated by statistical methods. The 2-mode model partially addresses the problem by only allowing it to affect the attribution of the deep mode, while the shallow mode is attributed to SC only. Nevertheless, the above limitation should not affect our conclusion about the constancy in SST_{rel}-P* and ∇^2SST-P* relationships (which js confirmed with independent analysis in Figure 2f) and that these relationships provide constraints on regional hydrological sensitivity.

Data Availability Statement

All observational and reanalysis data and the CMIP outputs used in this paper are publicly available at the following websites. CMIP (Eyring et al., 2016): https://esgf-node.llnl.gov/projects/cmip6/. GPCP (Adler et al., 2003): https://psl.noaa.gov/data/gridded/data.gpcp.html. CMAP (P. P. Xie & Arkin, 1997): https://www.psl.noaa.gov//data/gridded/data.cmap.html. TRMM (Huffman et al., 2010): https://disc.gsfc.nasa.gov/datasets/TRMM_3B43_7/summary. ERA5 (Hersbach et al., 2020): https://cds.climate.copernicus.eu/cdsapp#!/dataset/reanalysis-era5-pressure-levels-monthly-means?tab=form. NCEP/DOE-II (Kanamitsu et al., 2002): https://psl.noaa.gov/data/gridded/data.ncep.reanalysis2.html. JRA-55 (KOBAYASHI et al., 2015): https://jra.kishou.go.jp/JRA-55/index_en.html. The 2-mode coefficients and scripts used to analyze data and generate plots are stored in the Zenodo online repository at https://zenodo.org/records/11227083 He, Deng, et al. (2024).

Acknowledgments
We thank Drs. Robin Chadwick, Brian Soden and Bosong Zhang for helpful discussions. J.H. is supported by the National Science Foundation (NSF) grant AGS-2047270, B.F. is supported by NSF grant AGS-2217619, and Y.D. is supported by NSF grant AGS-2032532 and by the National Oceanic and Atmospheric Administration (NOAA) through Grants NA20OAR4310380 and NA22OAR4310606. We acknowledge the World Climate Research Programme's Working Group on Coupled Modelling, which is responsible for CMIP, and we thank the climate modelling groups for producing and making available their model output. For CMIP, the US Department of Energy's Program for Climate Model Diagnosis and Intercomparison provides coordinating support and led development of software infrastructure in partnership with the Global Organization for Earth System Science Portals. We thank the Physical Sciences Laboratory (PSL) of the National Oceanic and Atmospheric Administration and the Goddard Earth Sciences Data and Information Services Center for providing precipitation observations. We thank the Copernicus program, PSL, and the National Center for Atmospheric Research for providing the reanalysis data.

References

Adler, R. F., Huffman, G. J., Chang, A., Ferraro, R., Xie, P.-P., Janowiak, J., et al. (2003). The version-2 global precipitation Climatology project (GPCP) monthly precipitation analysis (1979–present). *Journal of Hydrometeorology*, *4*(6), 1147–1167. https://doi.org/10.1175/1525-7541(2003)004<1147:TVGPCP>2.0.CO;2

Back, L. E., & Bretherton, C. S. (2009a). A simple model of climatological rainfall and vertical motion patterns over the tropical oceans. *Journal of Climate*, *22*(23), 6477–6497. https://doi.org/10.1175/2009jcli2393.1

Back, L. E., & Bretherton, C. S. (2009b). On the relationship between SST gradients, boundary layer winds, and convergence over the Tropical Oceans. *Journal of Climate*, *22*(15), 4182–4196. https://doi.org/10.1175/2009JCLI2392.1

Chadwick, R. (2016). Which aspects of CO2 forcing and SST warming cause most uncertainty in projections of tropical rainfall change over land and ocean? *Journal of Climate*, *29*(7), 2493–2509. https://doi.org/10.1175/JCLI-D-15-0777.1

Chen, X., Zhou, T., Wu, P., Guo, Z., & Wang, M. (2020). Emergent constraints on future projections of the western north pacific subtropical high. *Nature Communications*, *11*(1), 2802. https://doi.org/10.1038/s41467-020-16631-9

Conn, A. R., Gould, N. I., & Toint, P. L. (2000). *Trust region methods*. SIAM.

DeAngelis, A. M., Qu, X., Zelinka, M. D., & Hall, A. (2015). An observational radiative constraint on hydrologic cycle intensification. *Nature*, *528*(7581), 249–253. https://doi.org/10.1038/nature15770

Duffy, M. L., O'Gorman, P. A., & Back, L. E. (2020). Importance of laplacian of low-level warming for the response of precipitation to climate change over Tropical Oceans. *Journal of Climate*, *33*(10), 4403–4417. https://doi.org/10.1175/JCLI-D-19-0365.1

Eyring, V., Bony, S., Meehl, G. A., Senior, C. A., Stevens, B., Stouffer, R. J., & Taylor, K. E. (2016). Overview of the coupled model Intercomparison project phase 6 (CMIP6) experimental design and organization. *Geoscientific Model Development*, *9*(5), 1937–1958. https://doi.org/10.5194/gmd-9-1937-2016

Good, P., Chadwick, R., Holloway, C., Kennedy, J., Lowe, J., Roehrig, R., & Rushley, S. (2020). High sensitivity of tropical precipitation to local sea-surface temperature.

Graham, N. E., & Barnett, T. P. (1987). Sea surface temperature, surface wind divergence, and convection over Tropical Oceans. *Science*, *238*(4827), 657–659. https://doi.org/10.1126/science.238.4827.657

Ham, Y.-G., Kug, J.-S., Choi, J.-Y., Jin, F.-F., & Watanabe, M. (2018). Inverse relationship between present-day tropical precipitation and its sensitivity to greenhouse warming. *Nature Climate Change*, *8*(1), 64–69. https://doi.org/10.1038/s41558-017-0033-5

He, J., Deng, Y., Fosu, B., Lin, Y.-H., & Lu, K. (2024). Constraining regional hydrological sensitivity over Tropical Oceans - Analysis. [Dataset]. https://doi.org/10.5281/zenodo.11227083. *Zenodo*.

He, J., Johnson, N. C., Vecchi, G. A., Kirtman, B., Wittenberg, A. T., & Sturm, S. (2018). Precipitation sensitivity to local variations in tropical sea surface temperature. *Journal of Climate*, *31*(22), 9225–9238. https://doi.org/10.1175/JCLI-D-18-0262.1

He, J., Lu, K., Fosu, B., & Fueglistaler, S. A. (2024). Diverging hydrological sensitivity among tropical basins. *Nature Climate Change*, *14*, 1–6. https://doi.org/10.1038/s41558-024-01982-8

He, J., & Soden, B. J. (2015). Anthropogenic weakening of the tropical circulation: The relative roles of direct CO2 forcing and sea surface temperature change. *Journal of Climate*, *28*(22), 8728–8742. https://doi.org/10.1175/JCLI-D-15-0205.1

Hersbach, H., Bell, B., Berrisford, P., Hirahara, S., Horányi, A., Muñoz-Sabater, J., et al. (2020). The ERA5 global reanalysis. *Quarterly Journal of the Royal Meteorological Society*, *146*(730), 1999–2049. https://doi.org/10.1002/qj.3803

Huffman, G. J., Adler, R. F., Bolvin, D. T., & Nelkin, E. J. (2010). The TRMM multi-satellite precipitation analysis (TMPA). In *Satellite rainfall applications for surface hydrology* (pp. 3–22). Springer.

Hurrell, J. W., Hack, J. J., Shea, D., Caron, J. M., & Rosinski, J. (2008). A new sea surface temperature and sea Ice boundary dataset for the community atmosphere model. *Journal of Climate*, *21*(19), 5145–5153. https://doi.org/10.1175/2008JCLI2292.1

Johnson, N. C., & Xie, S.-P. (2010). Changes in the sea surface temperature threshold for tropical convection. *Nature Geoscience*, *3*(12), 842–845. https://doi.org/10.1038/ngeo1008

Kanamitsu, M., Ebisuzaki, W., Woollen, J., Yang, S.-K., Hnilo, J., Fiorino, M., & Potter, G. (2002). Ncep–doe amip-ii reanalysis (r-2). *Bulletin of the American Meteorological Society*, *83*(11), 1631–1644. https://doi.org/10.1175/bams-83-11-1631(2002)083<1631:nar>2.3.co;2

Kent, C., Chadwick, R., & Rowell, D. P. (2015). Understanding uncertainties in future projections of seasonal tropical precipitation. *Journal of Climate*, *28*(11), 4390–4413. https://doi.org/10.1175/JCLI-D-14-00613.1

Kobayashi, S., Ota, Y., Harada, Y., Ebita, A., Moriya, M., Onoda, H., et al. (2015). The JRA-55 reanalysis: General specifications and basic characteristics. 気象集誌. 第2輯, *93*(1), 5–48. https://doi.org/10.2151/jmsj.2015-001

Kramer, R. J., & Soden, B. J. (2016). The sensitivity of the hydrological cycle to internal climate variability versus anthropogenic climate change. *Journal of Climate*, *29*(10), 3661–3673. https://doi.org/10.1175/jcli-d-15-0408.1

Lau, K.-M., Wu, H.-T., & Bony, S. (1997). The role of large-scale atmospheric circulation in the relationship between tropical convection and sea surface temperature. *Journal of Climate*, *10*(3), 381–392. https://doi.org/10.1175/1520-0442(1997)010<0381:TROLSA>2.0.CO;2

Lee, J.-Y., Marotzke, J., Bala, G., Cao, L., Corti, S., Dunne, J. P., et al. (2021). Future global climate: Scenario-based projections and near-term information. In *Climate change 2021: The physical science basis. Contribution of working group I to the sixth assessment report of the intergovernmental panel on climate change* (pp. 553–672). Cambridge University Press.

Lindzen, R. S., & Nigam, S. (1987). On the role of sea surface temperature gradients in forcing low-level winds and convergence in the tropics. *Journal of the Atmospheric Sciences*, *44*(17), 2418–2436. https://doi.org/10.1175/1520-0469(1987)044<2418:OTROSS>2.0.CO;2

Lu, K., He, J., & Simpson, I. R. (2023). Origins of uncertainty in the response of the summer north Pacific subtropical high to CO2 forcing. *Geophysical Research Letters*, *50*(22), e2023GL105042. https://doi.org/10.1029/2023gl105042

Ma, J., & Xie, S.-P. (2013). Regional patterns of sea surface temperature change: A source of uncertainty in future projections of precipitation and atmospheric circulation. *Journal of Climate*, *26*(8), 2482–2501. https://doi.org/10.1175/JCLI-D-12-00283.1

Park, I.-H., Yeh, S.-W., Min, S.-K., Ham, Y.-G., & Kirtman, B. P. (2022). Present-day warm pool constrains future tropical precipitation. *Communications Earth & Environment*, *3*(1), 310. https://doi.org/10.1038/s43247-022-00620-5

Su, H., Jiang, J. H., Neelin, J. D., Shen, T. J., Zhai, C., Yue, Q., et al. (2017). Tightening of tropical ascent and high clouds key to precipitation change in a warmer climate. *Nature Communications*, *8*(1), 15771. https://doi.org/10.1038/ncomms15771

Watanabe, M., Kamae, Y., Shiogama, H., DeAngelis, A. M., & Suzuki, K. (2018). Low clouds link equilibrium climate sensitivity to hydrological sensitivity. *Nature Climate Change*, *8*(10), 901–906. https://doi.org/10.1038/s41558-018-0272-0

Xie, P., & Arkin, P. A. (1997). Global precipitation: A 17-year monthly analysis based on gauge observations, satellite estimates, and numerical model outputs. *Bulletin of the American Meteorological Society*, *78*(11), 2539–2558. https://doi.org/10.1175/1520-0477(1997)078<2539:GPAYMA>2.0.CO;2

Xie, S.-P., Deser, C., Vecchi, G. A., Ma, J., Teng, H., & Wittenberg, A. T. (2010). Global warming pattern formation: Sea surface temperature and rainfall. *Journal of Climate*, *23*(4), 966–986. https://doi.org/10.1175/2009JCLI3329.1

Zhang, C. (1993). Large-scale variability of atmospheric deep convection in relation to sea surface temperature in the tropics. *Journal of Climate*, *6*(10), 1898–1913. https://doi.org/10.1175/1520-0442(1993)006<1898:LSVOAD>2.0.CO;2

Zhang, J., & Huang, P. (2023). Different uncertainty in tropical oceanic and land precipitation sensitivities under global warming. *Atmospheric Research*, *292*, 106850. https://doi.org/10.1016/j.atmosres.2023.106850